Nuclear Physics B122 (1977) 365–382

ω MESON PRODUCTION BY VIRTUAL PHOTONS

P. JOOS, A. LADAGE, H. MEYER ‡, P. STEIN ⋆, G. WOLF and S. YELLIN ⋆⋆
Deutsches Elektronen-Synchrotron DESY, Hamburg

C.K. CHEN ⋆⋆⋆, J. KNOWLES, D. MARTIN, J.M. SCARR, I.O. SKILLICORN and K. SMITH
University of Glasgow, Glasgow

C. BENZ, G. DREWS, D. HOFFMANN ‡, J. KNOBLOCH ‡‡, W. KRAUS, H. NAGEL, E. RABE, C. SANDER, W.-D. SCHLATTER ‡‡, H. SPITZER and K. WACKER ‡
II. Institut für Experimentalphysik der Universität Hamburg

Received 28 January 1977

Quasi-elastic ω production by ep scattering in the kinematic region $0.3 < Q^2 < 1.4$ GeV^2 and $1.7 < W < 2.8$ GeV was studied using a streamer chamber at DESY. The production angular distribution for $\gamma_V p \to \omega p$ has a strong non-peripheral component for $W < 2$ GeV. The ω production cross section falls by a factor of 4 as W changes from 1.7 to 2.8 GeV. In contrast the cross section for ω production with $|t| < 0.5$ GeV^2 is W independent between 1.7 and 2.8 GeV and for $W > 2.0$ GeV consistent in both W and Q^2 dependence with the predictions of a model based on one-pion exchange and diffraction.

1. Introduction

In this paper we present final results on quasi-elastic ω production from an experiment which used the DESY streamer chamber to study inelastic electron-proton scattering. The experiment covered hadron c.m.s. energies W between threshold and 2.8 GeV, and values of the photon mass squared, $-Q^2$ from -0.3 to -1.4 GeV^2. The experimental setup had nearly 4π acceptance for detection of charged hadrons. Here

‡ Now at Gesamthochschule Wuppertal.
⋆ On leave of absence from Cornell University, Ithaca, NY, USA.
⋆⋆ Now at University of California, Santa Barbara, California, USA.
⋆⋆⋆ Now at Argonne National Laboratory, Argonne, 111, USA.
‡ Now at Technische Hochschule Aachen, III, Physikalisches Institut A.
‡‡ Now at CERN, Geneva.

we give results on ω production by virtual photons *via*

$$\gamma_V p \to \omega p \,. \tag{1}$$

Final results on rho production and preliminary results on multiplicities and Δ^{++} production have already been published [1–5].

Reaction (1) provides an opportunity to study ω production as a function of the photon mass. At $Q^2 = 0$ the general characteristics of ω production have been determined through the use of a polarized photon beam. The polarized beam has permitted the measurement of the amount of natural and unnatural parity exchange in the t-channel [6]. It was found that the cross section associated with unnatural parity exchange has the $1/E_\gamma^2$ dependence characteristic of one-pion exchange (E_γ is the photon energy) while the natural parity exchange cross section is approximately constant as expected for a diffractive process. A model based on a combination of one-pion exchange (OPE) and diffraction is found to fit the data well [6,7]. One of the objects of this experiment is to determine if ω production by virtual photons can also be understood in terms of these mechanisms. To this end we have measured the cross section for reaction (1) and its dependence on Q^2, W and t. We find a large non-peripheral component of the ω cross section which cannot be explained by the contributions from OPE and diffraction alone.

The paper is organized as follows: first we review the experimental procedure. In sect. 3 we give the $\pi^+\pi^-\pi^0$ mass distribution for the channel $\gamma_V p \to p\pi^+\pi^-\pi^0$ and describe how the numbers of ω events were determined. In sect. 4 we discuss the ω production cross section as a function of W, Q^2 and t, and the ω decay distributions. The data are compared with an OPE-diffraction model in sect. 5. A summary is given in sect. 6.

2. Experimental procedure

A detailed description of the apparatus and the event analysis procedure has been given in ref. [2]. A 7.2 GeV electron beam was directed onto a 9 cm long liquid hydrogen target inside a streamer chamber. The streamer chamber, of 1 m length, was in an 18 kG magnetic field. Two arrays of trigger counters, lucite Čerenkov counters and lead scintillator sandwich shower counters detected the scattered electron. The present analysis is based on data taken with a proportional wire chamber added to each of the two detector arms [8]. The coordinate information from the chambers improved the momentum and angular resolution of the scattered electron by more than a factor two compared with the measurement of the electron in the streamer chamber only.

Approximately 200 000 pictures were taken with this setup. The integrated flux was $\sim 2 \times 10^{12}$ electrons. The photographs were scanned twice and ambiguities were resolved in a third scan. The procedure for the measurement of the film was similar to that used in bubble chamber experiments. Geometrical reconstruction and kine-

Table 1
Correction factors for fit losses due to measurement errors and due to external and internal bremsstrahlung

$\|t\|$ (GeV^2)	W(GeV)	
	1.7 – 2.0	2.0 – 2.8
0 – 0.1	–	1.38 ± 0.03
0.1 – 0.5	1.45 ± 0.04	1.26 ± 0.03
0.5 – 1.0	1.55 ± 0.05	1.40 ± 0.06
1.0 – 2.0	1.70 ± 0.07	1.47 ± 0.06
2.0 → t_{max}	2.0 ± 0.34	1.8 ± 0.07
all t	1.53 ± 0.05	1.40 ± 0.04

matical fitting were done using the programs THRESH and GRIND [9].

Omega meson production *via* reaction (1) was studied in the final state

$$ep \to ep\pi^+\pi^-\pi^0 \,. \tag{2}$$

The events selected as reaction (2) were required (a) to have a 1C fit (with $\chi^2 < 28$) consistent with the observed track ionization (b) to have *no* 4C fits of the type $ep \to ep\pi^+\pi^-$ consistent with the track ionization. A total of 2746 events satisfying these criteria were found in the kinematical region $1.7 < W < 2.8$ GeV, $0.3 < Q^2 < 1.4$ GeV^2.

In the determination of ω cross sections, corrections of approximately +40% have been applied for fit losses due to measurement errors and due to radiative effects (external and internal bremsstrahlung). The corrections were obtained from a Monte Carlo program which simulated the event production and detection in the streamer chamber. The Monte Carlo events were processed through GRIND in the same way as the measured events. It was found that events were lost for the following main reasons 14% – through bremsstrahlung causing the scattered electron to miss the trigger counters, 15.5% – no 1C fit, 10.5% – a 3C or 4C fit to $ep \to ep\pi^+\pi^-$. The correction factors, given in table 1, show some dependence on W and the four momentum transfer squared, t, between the initial and final state proton, but do not vary systematically with Q^2. An extra –7% correction was applied for vertex and propagator effects. Corrections of 11% and 10% *, respectively, were made for ω decays into neutrals [10] and ω events outside the 0.72–0.84 GeV mass interval.

Cross sections were determined by normalizing the total number of inelastic ep events (after correcting for acceptance and radiative effects) to the total inelastic ep cross section measured in a single arm experiment [11]. The errors quoted include

* The Monte Carlo events show the presence of non-Gaussian tails of the ω-resolution function, which contain 10% of the events (outside the interval 0.72–0.84 GeV).

the statistical error plus the uncertainty of the background subtraction under the ω. A systematic uncertainty of ±10% has to be added which covers the uncertainties from event selection, radiative corrections and cross section normalization.

3. Mass distribution for $\gamma_V p \to p\pi^+\pi^-\pi^0$

The $\pi^+\pi^-\pi^0$ mass spectra from reaction (2) are shown in figs. 1 and 2 for different Q^2 and W intervals. The shaded parts have a t-cut, $|t| < 0.5$ GeV^2. The ω peak is clearly seen at all energies. The numbers of ω's and hence the cross sections were determined using different procedures depending on the energy. For the lowest W interval, 1.7–2.0 GeV, the mass spectrum was fitted to a sum of ω production and three pion phase-space background. For the higher W intervals a fit was made to the mass interval 0.6–1.0 GeV with an ω contribution plus a second-order polynomial background.

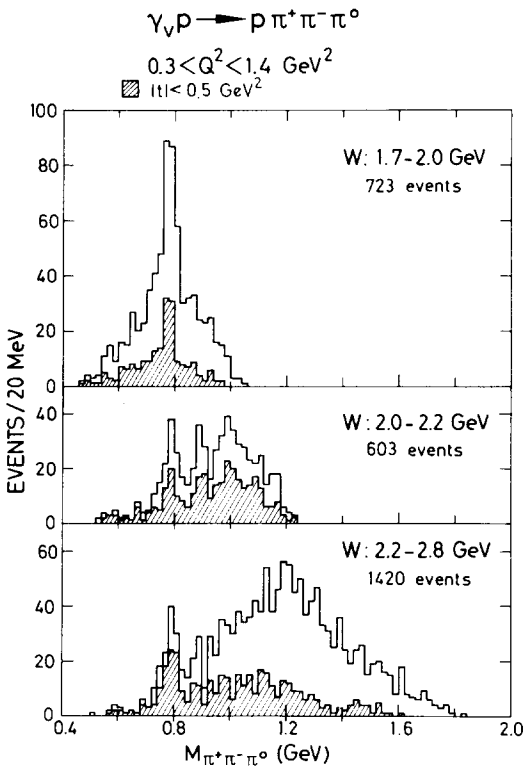

Fig. 1. Distribution of the effective mass $M_{\pi^+\pi^-\pi^0}$ from the reaction $ep \to ep\pi^+\pi^-\pi^0$ for $0.3 < Q^2 < 1.4$ GeV^2 and three W intervals. The shaded plots are for $|t| < 0.5$ GeV^2 where $|t|$ is the four-momentum transfer squared from γ to ω.

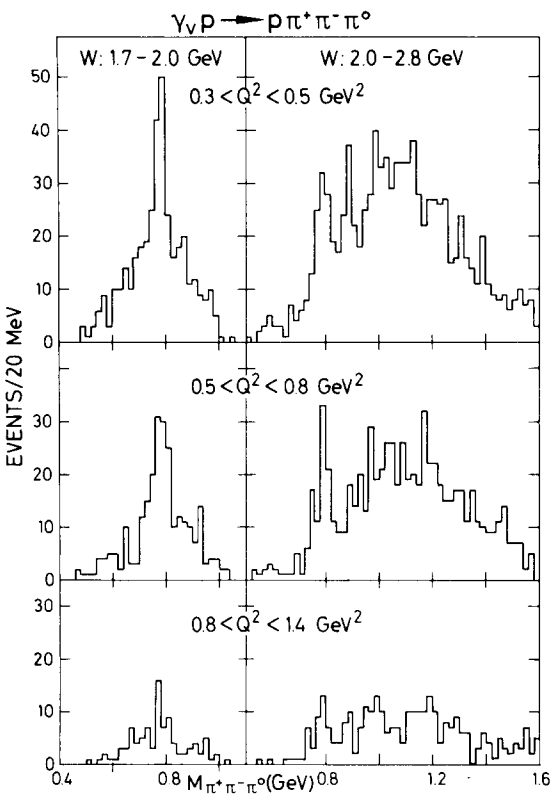

Fig. 2. Reaction $ep \to ep\pi^+\pi^-\pi^0$. Distribution of the effective mass $M_{\pi^+\pi^-\pi^0}$ for two W and three Q^2 intervals.

The ω peak was described in the fit by a Gaussian with an rms width of $\sim \pm 20$ MeV. In all cases the results of the fits were checked with estimates using hand-drawn backgrounds. For those intervals where the numbers of events were small only hand-drawn backgrounds were used.

4. The reaction $\gamma_V p \to \omega p$

4.1. Cross sections

Fig. 3 and table 2 show the W dependence of the ω cross section (a) for all values of $|t|$ and (b) for $|t| < 0.5$ GeV^2 ★; the latter cut was made to select peripherally

★ The definition of the $\gamma_V p$ cross section is given in the appendix.

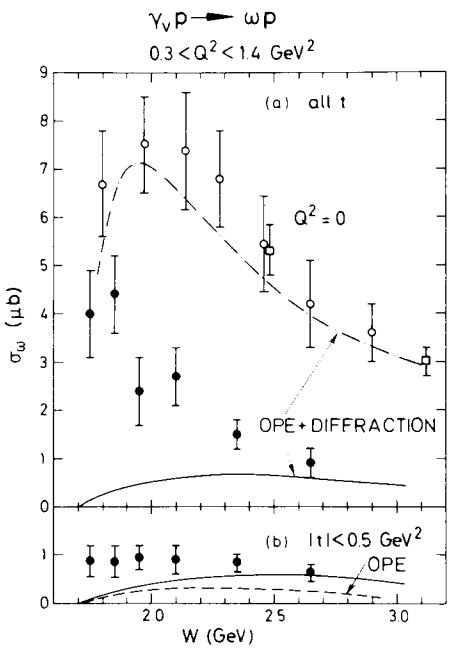

Fig. 3. $\sigma(\gamma_V p \to \omega p)$ for $0.3 < Q^2 < 1.4$ GeV^2 as a function of W. (a) for all t. (b) for $|t| < 0.5$ GeV^2. The open points are from the photoproduction data of ref. [6] (open squares) and ref. [7] (open circles). The curves are from the model discussed in sect. 5. The full and dash-dotted lines give the total contribution of the model; the dashed line gives the OPE part alone.

produced ω's. Comparison of figs. 3a and b shows that close to the ω threshold most of the cross section is due to non-peripheral ω production, which falls with increasing W. In contrast the peripheral ω production is approximately constant within $1.7 < W < 2.8$ GeV. The curves in fig. 3 will be discussed in sect. 5. The open points in fig. 3a are from photoproduction experiments [6,7].

Figs. 4a and b display the total and peripheral ω production cross section as a function of Q^2. A significant Q^2 dependence is seen only between $Q^2 = 0$ (open circles from refs. [6,7]) and $Q^2 = 0.3$ GeV^2 where σ_ω drops by a factor of 2–5. For comparison we show the ω cross sections from the SLAC μp streamer chamber experiment [12] (open squares).

Fig. 5 shows the production angular distribution in the $\gamma_V p$ center of mass system for $1.7 < W < 2.0$ GeV. Apart from a weak forward peak the bulk of the production cross section is nonperipheral. For $W > 2$ GeV the forward peak is more pronounced as can be seen from the differential cross section $d\sigma/dt$ in fig. 6 (full points). The electroproduction cross sections of figs. 5 and 6 are also listed in table 3. The open points in figs. 5 and 6 are from photoproduction experiments at comparable values of W [6,7]. For $|t| < 0.5$ GeV^2 ($\cos \Theta_{cm} > 0.6$) the electroproduction cross sections are lower by a factor of 3–4. In contrast the non-peripheral contributions for

Table 2
Reaction $\gamma_V p \to \omega p$: ω production cross section (in μb) as a function of Q^2 and W

		all t			$\|t\| < 0.5$ GeV^2	
W (GeV)	Q^2 (GeV^2)	$\langle Q^2 \rangle$ (GeV^2)	σ_ω	$\sigma_\omega/\sigma_{tot}$	$\langle Q^2 \rangle$ (GeV^2)	σ_ω
1.7 – 1.8		0.8	4.0 ± 0.9	0.047 ± 0.011	0.6	0.89 ± 0.33
1.8 – 1.9		0.8	4.4 ± 0.8	0.060 ± 0.011	0.6	0.86 ± 0.33
1.9 – 2.0		0.7	2.4 ± 0.7	0.035 ± 0.010	0.6	0.94 ± 0.26
2.0 – 2.2	0.3 – 1.4	0.9	2.7 ± 0.6	0.042 ± 0.009	0.6	0.90 ± 0.30
2.2 – 2.5		0.75	1.5 ± 0.3	0.026 ± 0.005	0.67	0.84 ± 0.18
2.5 – 2.8		0.75	0.9 ± 0.3	0.017 ± 0.006	0.74	0.63 ± 0.16
	0		7.0 ± 0.8	0.045 ± 0.005		4.2 ± 0.7
	0.3 – 0.5	0.4	3.9 ± 0.8	0.038 ± 0.008	0.39	1.46 ± 0.46
1.7 – 2.0	0.5 – 0.8	0.65	4.9 ± 0.9	0.058 ± 0.011	0.65	1.78 ± 0.43
$\langle W \rangle = 1.85$	0.8 – 1.4	1.05	2.8 ± 0.9	0.048 ± 0.015	0.92	0.32 ± 0.24
	0		7.4 ± 1.0	0.051 ± 0.007		5.3 ± 0.8
	0.3 – 0.5	0.4	2.1 ± 0.7	0.023 ± 0.008	0.42	0.54 ± 0.42
2.0 – 2.2	0.5 – 0.8	0.64	2.3 ± 0.7	0.032 ± 0.010	0.61	1.05 ± 0.40
$\langle W \rangle = 2.09$	0.8 – 1.4	1.20	3.0 ± 1.3	0.058 ± 0.025	0.90	0.94 ± 0.50
	0		5.4 ± 0.6	0.040 ± 0.004		4.4 ± 0.5
	0.3 – 0.5	0.42	1.1 ± 0.3	0.014 ± 0.004	0.43	0.93 ± 0.24
2.2 – 2.8	0.5 – 0.8	0.64	1.4 ± 0.4	0.023 ± 0.007	0.63	0.95 ± 0.24
$\langle W \rangle = 2.43$	0.8 – 1.4	1.0	1.0 ± 0.3	0.023 ± 0.007	0.94	0.58 ± 0.22

The data at $Q^2 = 0$ are from refs. [6,7]. For completeness we also give the ratio $\sigma_\omega/\sigma_{tot}$, where σ_{tot} was determined by a fit to the data of ref. [11].

$|t| > 0.5$ GeV^2 ($\cos\Theta_{cm} < 0.6$) decrease only by a factor ~1.5 between $Q^2 = 0$ and $\langle Q^2 \rangle = 0.7$ GeV^2.

4.2. ω decay angular distribution

The ω decay angular distribution * has been analysed in terms of the ω density matrix elements in the helicity system using the formalism of ref. [13]. The values of the density matrix elements are given in table 4 **. Only r^{04}_{00} differs significantly from

* We use the same formulae as in our study of ρ production [5]. The ω decay angles are defined as in the appendix of ref. [5] replacing the direction $\hat{\pi}^+$ of the π^+ from ρ decay by the normal $\hat{\pi}^+ \times \hat{\pi}^-$ to the ω decay plane in the ω rest system. The angular distributions $W(\cos\Theta_H)$ and $W(\psi_H)$ (not shown) are consistent with isotropy.

** The density matrix elements were determined by the method of moments from all events in the interval $0.72 < M_{\pi^+\pi^-\pi^0} < 0.84$ GeV. We have checked (from control regions) that the background does not change the results within the errors quoted.

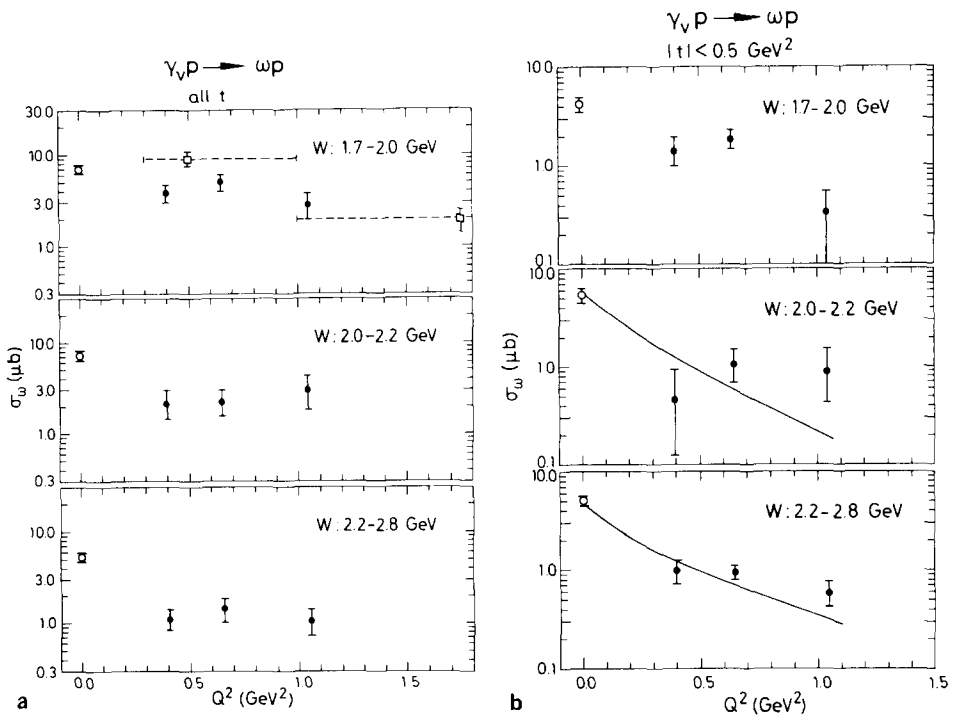

Fig. 4. $\sigma(\gamma_V p \rightarrow \omega p)$ as a function of Q^2 for different W intervals. (a) for all t. (b) for $|t| < 0.5$ GeV^2. The open circles at $Q^2 = 0$ are from refs. [6,7]. The open squares are data from ref. [12]. The curves are from the model discussed in sect. 5.

zero. We find no evidence that r_{00}^{04} is Q^2 dependent within the range $0.3 < Q^2 < 1.4$ GeV^2. The values of r_{00}^{04} found for peripheral ω's at both low and high W are, within errors, equal to those found in photoproduction [6,7]; this indicates that, in contrast to ρ electroproduction [5], there is no substantial increase in the production of longitudinal ω's when going from $Q^2 = 0$ to $\langle Q^2 \rangle = 0.7$ GeV^2.

In polarized photoproduction it has been possible to separate the contributions from natural and unnatural parity exchange in the t channel [6]. With unpolarized electrons and protons we can only determine a lower limit to the natural parity exchange part σ_T^N of the transverse ω production cross section σ_T from the relation (see subsect. 4.2 of ref. [13])

$$\sigma_T^N \geqslant \tfrac{1}{2}\{1 + (2r_{1-1}^1 - r_{00}^1)\}\sigma_T \,. \tag{3}$$

From the data of table 4 we obtain for $|t| < 0.5$ GeV^2 $\sigma_T^N \geqslant (0.6 \pm 0.1)\sigma_T$ for both $1.7 < W < 2.0$ GeV and $2.0 < W < 2.8$ GeV; i.e. more than half of the peripheral transverse cross section is due to natural parity exchange. A determination of the

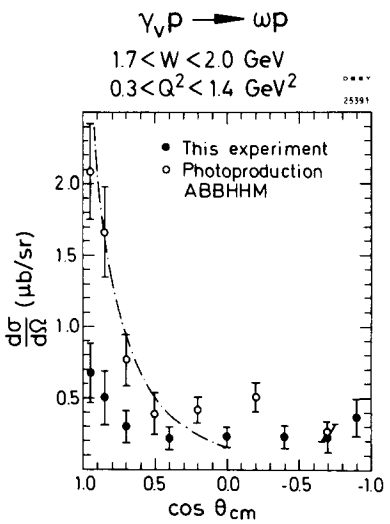

Fig. 5. $d\sigma/d\Omega$ ($\gamma_V p \rightarrow \omega p$) for $0.3 < Q^2 < 1.4$ GeV^2 and $1.7 < W < 2.0$ GeV. Θ_{cm} is the ω-production angle in the $\gamma_V p$ c.m. system. The open points are from the photoproduction data of ref. [7]. The curve is from the model discussed in sect. 5 (computed at $Q^2 = 0$).

longitudinal part is not possible within the present experiment; from the model discussed in sect. 5 one expects that only 10% of the unnatural parity exchange contribution (from one-pion exchange) are due to longitudinal photons.

4.3. Comparison of ω and ρ electroproduction

In figs. 7 and 8 we compare differential cross sections for ρ and ω production. At small production angles the ω cross section is smaller than the ρ cross section by a factor of 3–4. In the non-peripheral region ($|t| > 0.5$ GeV^2) the cross sections are approximately equal. The ratio of ω to ρ production as a function of Q^2 for different W intervals is shown in fig. 9 for all t. Within errors the ratio is Q^2 independent. For comparison we show the data of ref. [14] (open triangles) which are compatible with our data. Rho electroproduction has been found to be consistent with a dominantly diffractive process for $W > 2$ GeV [5]. If ω electroproduction were also dominated by diffraction * an ω to ρ cross section ratio of about 1 : 9 (corresponding to the ratio of the square of the $\gamma\omega$ and $\gamma\rho$ coupling constants) would be expected. We conclude from the data of figs. 7–9 that other mechanisms contribute to ω production, in particular for $|t| > 0.5$ GeV^2.

* We use the usual VDM picture, where the virtual photon couples to the ω meson with a subsequent diffractive ωp scattering.

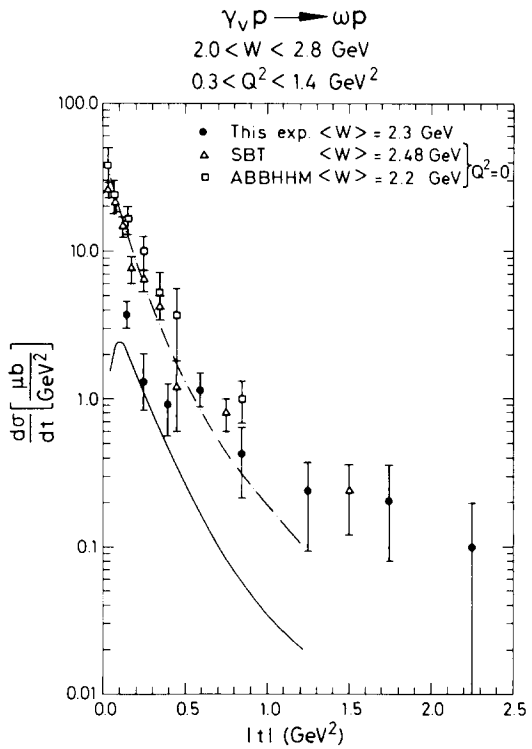

Fig. 6. $d\sigma/dt(\gamma_V p \to \omega p)$ for $0.3 < Q^2 < 1.4$ GeV^2 and $2.0 < W < 2.8$ GeV. The curves are from the model discussed in sect. 5. The points labelled SBT and ABBHHM are from the photoproduction data of refs. [6,7] respectively.

5. Comparison with a model

Photoproduction of ω mesons has been successfully explained by contributions from one-pion exchange and diffraction [6,7]. Starting from this Fraas [15] has developed a similar model for the electroproduction of ω mesons in which the production takes place through elementary one-pion exchange (OPE) and diffraction. We have modified his approach by including Benecke-Dürr form factors [16,17] in the OPE term and have used a diffractive term derived from photoproduction [6] so that at $Q^2 = 0$ the model fits photoproduction within 10%. We have used the value of $\Gamma_{\omega\to\pi\gamma} = 0.90$ MeV [10] for the radiative ω width and, following Fraas, have used the VDM relation $f_{\gamma\omega\pi}(Q^2) \propto [m_\rho^2/(m_\rho^2 + Q^2)]\, f_{\rho\omega\pi}$ for the relation between the $\gamma\omega\pi$ and $\rho\omega\pi$ coupling constants. The coupling constant $f_{\rho\omega\pi}$ could be Q^2 dependent but in the calculations presented here we have kept it constant at its $Q^2 = 0$ value. The basic formulae of the model are given in the appendix.

The curves of figs. 3, 4b and 6 show the predictions of the model. The dashed line

Table 3
Reaction $\gamma_V p \to \omega p$ at $0.3 < Q^2 < 1.4$ GeV^2: Differential cross sections $d\sigma/d\Omega$ (in the hadron c.m.s.) for $1.7 < W < 2.0$ GeV and $d\sigma/dt$ for $2.0 < W < 2.8$ GeV

$\langle Q^2 \rangle$ (GeV^2)	W(GeV)	$\cos \Theta_{cm}$	$d\sigma/d\Omega$ (μb/sr)
		0.9 – 1.0	0.68 ± 0.21
		0.8 – 0.9	0.50 ± 0.19
		0.6 – 0.8	0.30 ± 0.11
0.77	1.7 – 2.0	0.2 – 0.6	0.22 ± 0.08
		(–0.2) – 0.2	0.23 ± 0.07
	$\langle W \rangle$ = 1.84	(–0.6) – (–0.2)	0.23 ± 0.08
		(–0.8) – (–0.6)	0.23 ± 0.11
		(–1.0) – (–0.8)	0.37 ± 0.13
$\langle Q^2 \rangle$	W(GeV)	$\lvert t \rvert$ (GeV^2)	$d\sigma/dt$ (μb/GeV^2)
		< 0.1	*
		0.1 – 0.2	3.8 ± 0.8
		0.2 – 0.3	1.4 ± 0.6
0.84	2.0 – 2.8	0.3 – 0.5	0.90 ± 0.37
	$\langle W \rangle$ = 2.3	0.5 – 0.7	1.20 ± 0.36
		0.7 – 1.0	0.42 ± 0.23
		1.0 – 1.5	0.24 ± 0.15
		1.5 – 2.0	0.22 ± 0.14
		2.0 – 2.5	0.10 ± 0.10

* We have a signal of 20 ± 5.5 events corresponding to a cross section of 0.2 μb. We do not quote a differential cross section, since t_{min} varies drastically in the Q^2 and W interval considered.

in fig. 3b gives the contribution from OPE alone. For $W > 2$ GeV and $|t| < 0.5$ GeV^2 the model is in reasonable agreement with the data. However, for $W < 2$ GeV there is substantial ω production which is non-peripheral and nearly isotropic, and which shows a weak Q^2 dependence; these features cannot be explained by the model. This is in contrast to photoproduction for which the model gives a good description down to threshold (see dash-dotted curves in figs. 3a, 5 and 6). Hence we conclude that an additional production mechanism e.g. formation of s-channel resonances contributes strongly in ω electroproduction for $W < 2$ GeV.

6. Summary

We have measured the cross section for ω production by virtual photons as a function of Q^2, W and t. We find:

(i) ω production near threshold is dominantly non-peripheral (fig. 5). Some non-peripheral production persists at higher energies (fig. 6).

Table 4
Spin density matrix elements for $\gamma_V p \to \omega p$ in the s-channel helicity system ($0.3 < Q^2 < 1.4\,\mathrm{GeV}^2$)

	$\lvert t\rvert < 0.5\ \mathrm{GeV}^2$		all $\lvert t\rvert$	
W(GeV)	1.7 – 2.0	2.0 – 2.8	1.7 – 2.0	2.0 – 2.8
r^{04}_{00}	0.27 ± 0.07	0.28 ± 0.06	0.35 ± 0.04	0.24 ± 0.06
Re r^{04}_{00}	0.01 ± 0.04	0.07 ± 0.04	0.00 ± 0.03	−0.01 ± 0.03
r^{04}_{00}	−0.02 ± 0.06	0.13 ± 0.06	−0.08 ± 0.03	0.05 ± 0.04
r^{1}_{00}	−0.03 ± 0.12	−0.16 ± 0.09	−0.01 ± 0.06	−0.06 ± 0.07
r^{1}_{11}	−0.01 ± 0.07	0.12 ± 0.07	−0.05 ± 0.04	0.04 ± 0.05
Re r^{1}_{10}	−0.07 ± 0.06	−0.01 ± 0.06	0.04 ± 0.04	0.03 ± 0.04
r^{1}_{1-1}	0.09 ± 0.09	0.01 ± 0.10	0.02 ± 0.05	0.03 ± 0.07
Im r^{2}_{10}	−0.03 ± 0.07	0.02 ± 0.07	−0.02 ± 0.04	0.01 ± 0.05
Im r^{2}_{1-1}	0.07 ± 0.10	0.01 ± 0.09	0.04 ± 0.05	0.00 ± 0.06
r^{5}_{00}	0.08 ± 0.06	0.04 ± 0.05	0.05 ± 0.03	0.02 ± 0.04
r^{5}_{11}	0.01 ± 0.04	−0.00 ± 0.03	0.03 ± 0.02	0.01 ± 0.02
Re r^{5}_{10}	0.01 ± 0.03	0.02 ± 0.03	0.01 ± 0.02	0.01 ± 0.02
r^{5}_{1-1}	−0.07 ± 0.04	−0.06 ± 0.03	−0.05 ± 0.02	−0.04 ± 0.03
Im r^{6}_{10}	−0.06 ± 0.03	−0.01 ± 0.03	−0.03 ± 0.02	−0.02 ± 0.02
Im r^{6}_{1-1}	0.00 ± 0.05	−0.01 ± 0.04	0.01 ± 0.02	0.00 ± 0.03

(ii) The non-peripheral component is weakly Q^2 dependent and strongly energy dependent. It is responsible for the decrease of the total ω cross section from ~4 μb at threshold to ~1 μb at W = 2.8 GeV (see fig. 3).

(iii) The peripheral component of ω production ($|t| < 0.5\ \mathrm{GeV}^2$) is essentially energy independent in the range $1.7 < W < 2.8$ GeV. For $W > 2$ GeV its Q^2 and W dependence is compatible with a model based on VDM-modified OPE and diffraction (figs. 3b, 4b, 6).

(iv) The value of r^{04}_{00} for peripheral ω's is consistent with that found in photoproduction, indicating that, in contrast to ρ electroproduction, there is little increase in the production of longitudinal ω's when Q^2 changes from 0 to 0.7 GeV^2.

(v) Within errors the ratio $\sigma_\omega/\sigma_\rho$ is independent of Q^2 for $0 < Q^2 < 0.8\ \mathrm{GeV}^2$ and $W < 2.8$ GeV (fig. 9). At large $|t|$ the ω cross section is approximately equal to the ρ cross section (figs. 7, 8).

In conclusion: ω production by virtual photons in the kinematical region $1.7 < W < 2.8$ GeV and $Q^2 < 1.4\ \mathrm{GeV}^2$ has two main contributions: a non-peripheral part, which is strongly energy dependent, suggestive of s-channel resonance formation,

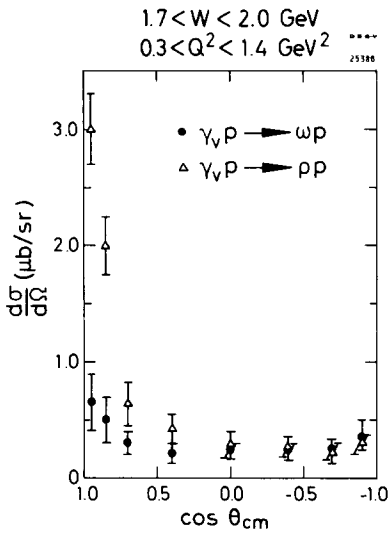

Fig. 7. Differential cross sections $d\sigma/d\Omega$ in the hadronic c.m.s. for reactions $\gamma_V p \to \omega p$ (full points) and $\gamma_V p \to \rho^0 p$ (open triangles from ref. [5]) for $1.7 < W < 2.0$ GeV and $0.3 < Q^2 < 1.4$ GeV^2.

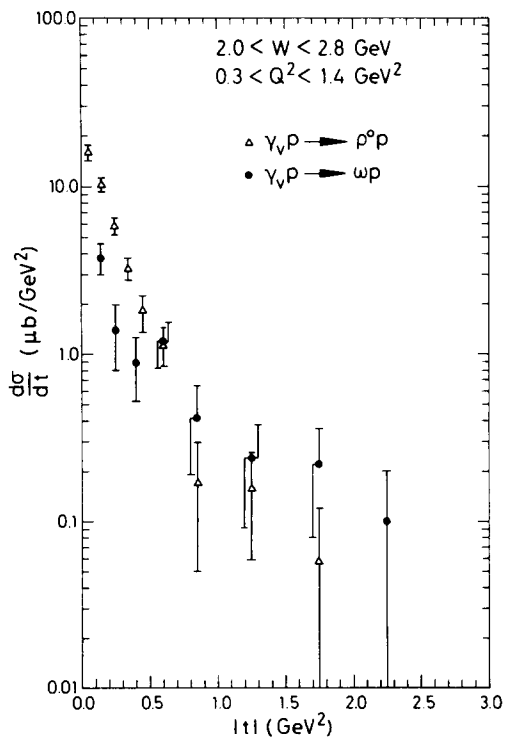

Fig. 8. Differential cross sections $d\sigma/dt$ for reactions $\gamma_V p \to \omega p$ (full points) and $\gamma_V p \to \rho^0 p$ (open triangles from ref. [5]) for $2.0 < W < 2.8$ GeV and $0.3 < Q^2 < 1.4$ GeV^2.

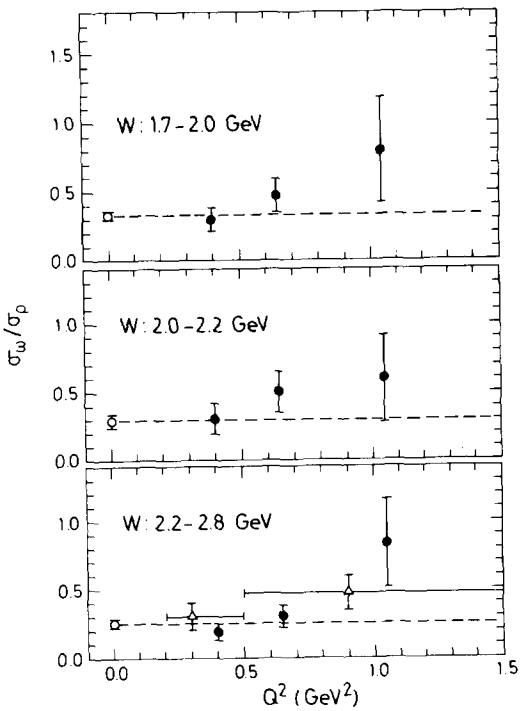

Fig. 9. The ratio $\sigma(\gamma_V p \to \omega p)/\sigma(\gamma_V p \to \rho p)$ as a function of Q^2 for different W intervals. The open circles and the dashed lines indicate the photoproduction values, which were taken from refs. [6,7]. The open triangles are data from ref. [14] for $2.0 < W < 5$ GeV with an average $\langle W \rangle = 2.65$ GeV.

and a peripheral part, consistent with a production mechanism *via* OPE and diffraction.

We thank I. Bloodworth, B. Naroska, D. Notz and W.J. Podolsky for their contributions in the early stages of this experiment. We are indebted to N. Gollmer, E. Hell, V. Heynen, A. Huber, K. Klinkmüller, G. Kraft, H.H. Sabath, S.W. Sass, K. Westphal, and K.H. Wroblewski, for technical assistance. The excellent performance of the Synchrotron crew, of the Hallendienst and of the Kältetechnik is gratefully acknowledged. We want to thank our scanning and measuring personnel for their careful work. The cooperation by Mr. Kuhlmann and the Rechenzentrum has been very helpful. The work at Hamburg has been supported by the Bundesministerium für Forschung und Technologie. The work at Glasgow has been supported by the Science Research Council.

Appendix

Differential cross section for the electroproduction of ω mesons

Definition of virtual photon cross sections

Following Hand [18] the differential cross section $d^2\sigma/dQ^2dW$ for electroproduction of ω's can be expressed in terms of σ_T and σ_L, which refer to ω production by transverse and longitudinal photons, respectively, using

$$\frac{d^2\sigma}{dQ^2 dW d|t|} = \frac{\pi}{EE'} \frac{W}{m_p} \Gamma_T \left\{ \frac{d\sigma_T}{d|t|} + \frac{\epsilon d\sigma_L}{d|t|} \right\}.$$

Here E, E' are the energies of the incident and scattered electron, m_p is the mass of the proton, Γ_T measures the flux of transverse photons and t is the four-momentum transfer squared from γ to ω.

$$\Gamma_T = \frac{\alpha}{4\pi^2} \frac{E'}{E} \frac{W^2 - m_p^2}{m_p Q^2} \frac{1}{1-\epsilon},$$

with

$$\epsilon = \left[1 + 2 \frac{\nu^2 + Q^2}{4EE' - Q^2} \right]^{-1},$$

$\nu = E - E'$,

W = hadron c.m.s. energy,

$-Q^2$ = photon mass squared.

Model for ω production cross sections

(a) One-pion-exchange contribution. Here we follow closely the equations of Fraas [15], but we introduce the Benecke-Dürr form-factors [16,17] which are found necessary to describe ω photoproduction [6].

For transverse photons the differential cross section, $d\sigma_T^\pi/dt$, is given by

$$d\sigma_T^\pi/dt = \frac{1}{P(Q^2)P(0)W^2} G^2 \frac{\Lambda_{\omega\pi}^2}{16} \frac{-t}{(t-m_\pi^2)^2} \frac{m_\rho^4}{(Q^2+m_\rho^2)^2} \times \frac{4(B+C)^2 - 2Q^2N_3^2}{4(-C)} F_N F_\omega,$$

while for longitudinal photons the corresponding expression is

$$d\sigma_L^\pi/dt = \frac{1}{P(Q^2)P(0)W^2} G^2 \frac{\Lambda_{\omega\pi}^2}{16} \frac{-t}{(t-m_\pi^2)^2} \frac{m_\rho^4}{(Q^2+m_\rho^2)^2} \frac{Q^2N_3^2}{(-C)} F_N F_\omega,$$

where G^2 is the square of the pion-nucleon coupling = 14.6,

$$\Lambda^2_{\omega\pi} = 96\pi \left(\frac{m_\omega}{(m_\omega^2 - m_\pi^2)}\right)^3 \Gamma_{\omega\pi\gamma} ,$$

with $\Gamma_{\omega\pi\gamma}$ being the partial width for $\omega \to \pi\gamma$, $\Gamma_{\omega\pi\gamma} = 0.9$ MeV; $P(0)$, $P(Q^2)$ are the photon momenta in the hadron c.m.s. for real and virtual photons, respectively; m_π, m_ρ, m_ω are the masses of the π, ρ and ω respectively; F_N, F_ω are the form-factors [17] for the π-nucleon and $\gamma\pi\omega$ vertices respectively with:

$$F_N = (1 + (2.9)^2 Q_N^2)/(1 + (2.9)^2 Q_{NT}^2)$$

where

$$Q_N^2 = m_\pi^2(m_\pi^2 - 4m_p^2)/(4m_p^2) ,$$

$$Q_{NT}^2 = t(t - 4m_p^2)/(4m_p^2) ,$$

$$F_\omega = U(2.3\,QF)/U(2.3\,QT)\,(QT/QF)^2 ,$$

where

$$U(x) = \left[\frac{2x^2 + 1}{4x^2} \log(4x^2 + 1) - 1\right]/(2x^2) ;$$

QT is the momentum of the on-shell pion (or γ) in the ω rest frame and QF is the momentum of the off-shell pion (or γ) in the ω rest frame.

The quantities B, C, N_3 are as defined by Fraas, namely,

$$B = -0.5\,Q^2(t - 2m_p^2) + 0.25(m_p^2 - Q^2 - W^2)(m_p^2 + m_\omega^2 - W^2 - t) ,$$

$$C = -0.25\{(W - m_p)^2 + Q^2\}\{(W + m_p)^2 + Q^2\} ,$$

$$N_3 = 0.5\{W^2 tu - t(m_p^2 + Q^2)(m_p^2 - m_\omega^2) - m_p^2(Q^2 + m_\omega^2)^2\}^{1/2} ,$$

with

$$W^2 + t + u = 2m_p^2 - Q^2 + m_\omega^2 .$$

(b) Diffraction contribution. We use a parametrisation for the diffractive ω cross section σ_D which is based on vector dominance and which at $Q^2 = 0$, fits the SLAC-LBL-Tufts data on ω production [6]

$$\sigma_D(\mu b) = \frac{P(0)}{P(Q^2)} (1 + \epsilon R) \frac{m_\omega^4}{(Q^2 + m_\omega^2)^2} \; 9.3(\exp(6.7\,t)) \left(1 + \frac{1.4}{E_\gamma}\right),$$

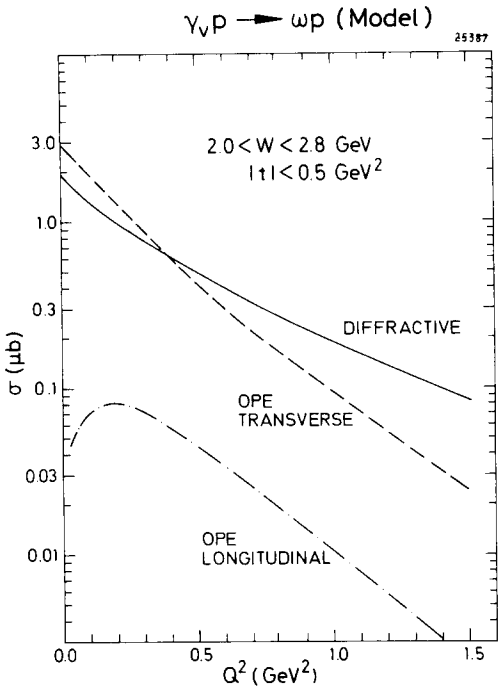

Fig. 10. Q^2 dependence of the diffractive (full curve), the transverse OPE (dashed curve) and the longitudinal OPE (dash-dotted curve) ω cross section as predicted by the model of sect. 5 for $2.0 < W < 2.8$ GeV and $|t| < 0.5$ GeV^2.

where

$$E_\gamma = (W^2 - m_p^2)/2m_p \,,$$

$$R = 0.4\, Q^2/m_\rho^2 \,,$$

and $P(0)/P(Q^2)$ takes account of the difference in photon flux for different Q^2 at a given W.

Fig. 10 illustrates the relative magnitude and Q^2 dependence of the diffractive, the transverse OPE and the longitudinal OPE contributions to the cross sections from the above model for $|t| < 0.5$ GeV^2 and $2.0 < W < 2.8$ GeV.

References

[1] V. Eckardt et al., Phys. Letters 43B (1973) 240; Nuovo Cimento Letters 6 (1973) 551.
[2] V. Eckardt et al., Nucl. Phys. B55 (1973) 45;

E. Rabe, Thesis, Internal report DESY F1-74/2 (1974), unpublished;
K. Wacker, Thesis, Internal report DESY F1-76/04 (1976), unpublished.
[3] V. Eckardt et al., DESY report 74/5 (1974), unpublished.
[4] P. Joos et al., Phys. Letters 52B (1974) 481; 62B (1976) 230.
[5] P. Joos et al., Nucl. Phys. B113 (1976) 53.
[6] J. Ballam et al., Phys. Rev. D7 (1973) 3150.
[7] ABBHHM Collaboration, Phys. Rev. 175 (1968) 1669.
[8] C. Sander, Diploma Thesis, Internal report DESY F1-75/3 (1975), unpublished.
[9] CERN TC-Library.
[10] Review of Particle Properties, Phys. Letters 50B (1974) 1.
[11] S. Stein et al., Phys. Rev. D12 (1975) 1884.
[12] R.F. Mozley, Proc. 1975 Int. Symp. on lepton and photon interactions at high energies, Stanford University (1975) p. 783;
B. Lieberman, Thesis, University of California at Santa Cruz (1975).
[13] K. Schilling and G. Wolf, Nucl. Phys. B61 (1973) 381.
[14] J. Ballam et al., Phys. Rev. D10 (1974) 765.
[15] H. Fraas, Nucl. Phys. B36 (1972) 191.
[16] J. Benecke and P.H. Dürr, Nuovo Cimento 56A (1968) 269.
[17] G. Wolf, Phys. Rev. 182 (1969) 1538.
[18] L. Hand, Phys. Rev. 129 (1964) 1834.